Power Quality Control for Grid Connected Photovoltaic System with Neutral Point Converter

Mehdi Et-taoussi [1*], Hamid Ouadi [1]

LPMMAT Laboratory, Physics Department, Faculty of Sciences Aïn Chock Hassan II-University of Casablanca
Casablanca, Morocco
[*] Corresponding Author: mehdiettaoussi@rocketmail.com

Abstract— **The problem of interfacing a Photovoltaic Generator (PVG) with an electrical three phase grid is addressed in the presence of nonlinear loads. The connection of the PVG to the power grid is done in two stages with both a DC/DC converter and DC/AC multilevel inverter. This latter is based on a Neutral Point Converter (NPC) operating simultaneously as an interfacing system and as a shunt active power filter. The main objectives of the proposed control system are threefold: (i) transferring the optimal power from PVG to the power grid; (ii) cancelling the load current harmonics and compensating the reactive power absorbed by nonlinear loads; (iii) balancing the capacitor voltages and regulating the DC bus voltage. To this end, two closed loops of nonlinear control are developed on the basis of the averaged PV system model. The control system includes firstly an AC current controller, designed with the Backstepping control technique, and using p-q Theory for the computation of these reference signals. Secondly, a DC bus voltage controller is designed using the sliding mode control technique. Simulations show that the proposed control system achieved the listed objectives under a widely varying load and solar irradiance levels.**

Keywords- PV Generator; 3-Level NPC Inverter; Shunt Active Power Filter; Backstepping Control Design; Sliding Mode Control.

I. INTRODUCTION

Nowadays, with the development of control tools, PV systems are no longer limited to active power generators in transmission and distribution networks, but they also contribute to the improvement of quality of the generated electrical energy (e.g. compensation of reactive load power and cancellation of current load harmonics) [1].

In the present study, the considered PV system is illustrated by Fig.1. In this system, the PV side converter is controlled to ensure the tracking of the maximum power point (MPPT) [2]. However, the grid side converter ensures the adjustment of the exchange of energy between the PV system and the power grid. Moreover, the latter converter can also meet the requirements of the quality standards of the produced electrical power [2]. Indeed, the widespread use of nonlinear loads in power systems causes circulation of harmonics and reactive currents in the distribution lines. Therefore, there is a degradation of produced power quality indicators (e.g. PFC, THD). Thus, additional losses occur in the transmission lines causing malfunction, both for the energy supplier and consumers [3]. To avoid these problems, the grid side converter (DC/AC) must be controlled to ensure, on the one hand, the control of the PV/Grid power exchange, and the quality control of the energy produced by the whole PV grid connected system on the other.

The control of the PV side converter (ensuring MPPT objective) has been widely discussed in the literature [2]. It should be noted that this study will not be the subject of this paper. However, the focus will be on the control of the grid side converter. As described in Fig.1, the considered converter is of a Diode-Clamped multilevel structure (NPC). Compared to the conventional two level structure [4], the multilevel inverter generates AC currents and voltages having a lower harmonic distortion. In addition, for a given power, the constraints on the multilevel inverter switches are less hard than in the case of a two level inverter. Indeed, for high power applications, the cost of the multilevel inverter is much lower. In addition, this inverter can also reduce abrupt variations in the AC output voltage. This will avoid some problems of electromagnetic compatibility [5].

Moreover, to ensure a proper connection of the PV system to the grid, some constraints must be taken into account at the NPC control design. In fact, the technical challenge is to balance the two capacitor voltages [6]. However, any inequality of the capacitor voltages leads to even harmonics in the NPC output voltage due to asymmetry [6].

The control problem of the grid side converter in a grid connected PV system has been addressed in several previous works (e.g. [7,8]). However, these works were limited to the simple case of a two level inverter structure. Furthermore, on the basis of the controller design technique, the previous works involving a multilevel NPC inverter for connecting a PV system to the power grid can be classified into two categories. The first one includes controllers using hysteresis operators or fuzzy logic (e.g. [9,10]). These methods do not take account of the exact nonlinear PV system model in the control design. Accordingly, the obtained controllers are not supported by formal stability analysis. In addition to achieve good tracking performances, these techniques generally lead to a variable and relatively high switching frequency [11]. This causes an inverter lifetime reduction, a switching losses increase and consequently degrades the PV system efficiency. The second category concerns the linear control techniques (e.g. [9,12]). Indeed, over a wide range variation of the operating point, the optimal performances are no longer achieved due to the nonlinear nature of the controlled system.

In this paper, a new nonlinear control system is designed for a 3-level NPC inverter ensuring the grid connection of PV system with power quality improvement. The involved nonlinear control laws are designed based on the Lyapunov's Stability Theory. The control system thus developed is illustrated by Fig.2. This multi-loop control involves a DC bus voltage controller, a balance controller (of the capacitor voltages) and an AC current controller. The extraction of the

978-1-5090-5713-9/16/$31.00

current references needed to the AC current control are carried out by the instantaneous power technique (p-q Theory). This technique has the advantage of being relatively fast and simple to be implemented [13].

This paper is organized as follows: the proposed grid connected PV system is described in Section II; while the grid connected PV system model is presented in Section III. In Section IV, the control system synthesis and analysis are presented. In Section V, the performances of the control system are illustrated by simulation considering various solar irradiance levels with different nonlinear loads. Section VI concludes the paper.

Table I. List of Notations

Notation	Designation
v_{ga}, v_{gb}, v_{gc}	Power grid voltages
V_{gd}, V_{gq}	Power grid voltages in d-q coordinates
$V_{g\alpha}, V_{g\beta}$	Power grid voltages in α-β coordinates
i_{ga}, i_{gb}, i_{gc}	Power grid currents
$v_{NPC\_a}, v_{NPC\_b}, v_{NPC\_c}$	NPC voltages
V_{NPC_d}, V_{NPC_q}	NPC voltages in d-q coordinates
$i_{NPC\_a}, i_{NPC\_b}, i_{NPC\_c}$	NPC currents
I_{NPC_d}, I_{NPC_q}	NPC currents in d-q coordinates
$i_{NL\_a}, i_{NL\_b}, i_{NL\_c}$	Nonlinear load currents
$I_{NL\_\alpha}, I_{NL\_\beta}$	Load currents in α-β coordinates
i_{pa}, i_{pb}, i_{pc}	NPC current active components
I_{pd}, I_{pq}	NPC current active components (d-q)
I_{s0}	PVG current
V_{bus}	DC bus voltage
V_{bus_1}, V_{bus_2}	DC capacitor voltages
R_d	Decoupling filter resistor
L_d	Decoupling filter inductance
C_{NPC}	NPC capacitor
V_g	RMS grid voltage
f_g	Power grid frequency

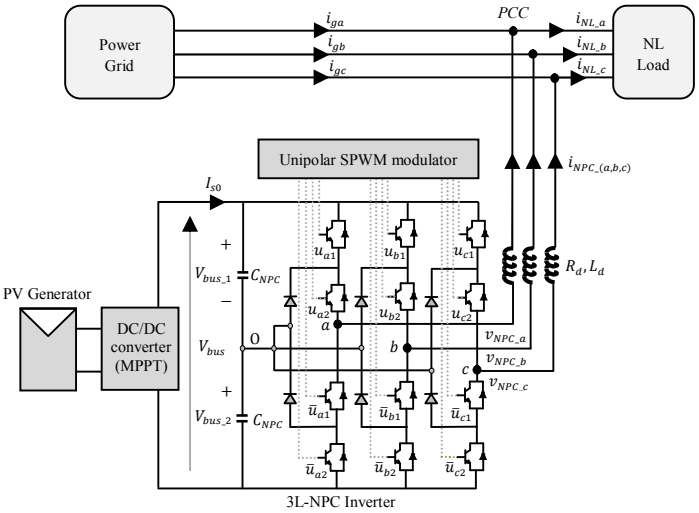

Figure 1. Electrical PV System Structure.

II. GRID CONNECTED PHOTOVOLTAIC SYSTEM DESCRIPTION

The present work focuses on the grid connected PV system described by Fig.1. This system consists of a Photovoltaic Generator (PVG) connected to the power grid through a DC/DC converter and a 3-level NPC inverter. Fig.1 shows that each arm of the inverter consists of four switches. The DC bus is fitted with a capacitive divider to provide two voltage sources of value $V_{bus}/2$ [12]. An inductor filter (R_d, L_d) is placed between the NPC inverter and the power grid in order to prevent the circulation of the current harmonics due to the NPC inverter switching [13]. The unipolar Sinusoidal Pulse Width Modulation (SPWM) is used to generate the gate signals for the NPC inverter [6].

III. GRID CONNECTED PHOTOVOLTAIC SYSTEM MODELING

The considered PV system is presented in Fig.1. It acts as a controlled current source connected in parallel with the nonlinear load at the PCC. To develop the inverter model, some assumptions are crucial:

A.1 The inverter power losses are assumed to be neglected.
A.2 For the SPWM, the carrier frequency is assumed to be much larger than that of the modulating signal.
A.3 The nonlinear loads as well as the utility grid are assumed to be balanced.

With assumption A.2, and neglecting high frequency harmonics of the modulating signal, the average value of the switching function $sw_a(t)$ can be approximated by the instantaneous value of the modulating signal as follows [6]:

$$sw_a(t) = +M\sin(\omega t + \theta) + \delta \quad \text{(for the first half cycle)} \quad (1)$$
$$sw_a(t) = -M\sin(\omega t + \theta) + \eta \quad \text{(for the second half cycle)} \quad (2)$$

where M, θ and ω are respectively the amplitude, the initial phase and the fundamental frequency of the modulating signal. Furthermore, δ and η are the DC offsets on each half cycle of the control signal $(sw_{(a,b,c)})$.

Remark 1

i. The switching function described by (1,2) concern the phase-a. The switching functions sw_b and sw_c are respectively obtained by shifting sw_a by $-2\pi/3$ and $-4\pi/3$.

ii. The inverter AC currents and voltages ($i_{NPC\_(a,b,c)}(t)$ and $v_{NPC\_(a,b,c)}(t)$) are approximated by their first harmonics. For example, the approximation of the inverter AC current phase-a leads to:

$$i_{NPC\_a}(t) = \langle i_{NPC\_a}\rangle_0 + \langle i_{NPC\_a}\rangle_{-1}e^{-j\omega t} + \langle i_{NPC\_a}\rangle_1 e^{j\omega t} \quad (3)$$

where $\langle i_{NPC\_a}\rangle_k$; $(k \in \{0,1,-1\})$ are the Fourier series development coefficients.

By applying the usual electrical laws to the PV/Grid connected system, with the notations of Table I, the NPC inverter dynamic can be described in the dq frame by the following generalized average model [6]:

$$\frac{dI_{NPC\_d}}{dt} = -\frac{R_d}{L_d}I_{NPC\_d} + \omega I_{NPC\_q} - \frac{1}{L_d}V_{gd} + \frac{1}{L_d}\left[V_{bus\_1}\left(\frac{M}{2}+\frac{2\delta}{\pi}\right) + V_{bus\_2}\left(\frac{M}{2}+\frac{2\eta}{\pi}\right)\right]\cos(\Lambda) \quad (4)$$

$$\frac{dI_{NPC\_q}}{dt} = -\frac{R_d}{L_d}I_{NPC\_q} - \omega I_{NPC\_d} - \frac{1}{L_d}V_{gq} + \frac{1}{L_d}\left[V_{bus\_1}\left(\frac{M}{2}+\frac{2\delta}{\pi}\right) + V_{bus\_2}\left(\frac{M}{2}+\frac{2\eta}{\pi}\right)\right]\sin(\Lambda) \quad (5)$$

$$\frac{d(V_{bus\_1}+V_{bus\_2})}{dt} = \frac{2}{C_{NPC}}\langle I_{s0}\rangle_0 - \frac{3}{2C_{NPC}}M\left(I_{NPC\_d}\cos(\Lambda) + I_{NPC\_q}\sin(\Lambda)\right) - \frac{3}{\pi C_{NPC}}\left(I_{NPC\_d}\cos(\Lambda) + I_{NPC\_q}\sin(\Lambda)\right)(\delta+\eta) \quad (6)$$

$$\frac{d(V_{bus\_1}-V_{bus\_2})}{dt} = -\frac{3}{\pi C_{NPC}}\left(I_{NPC\_d}\cos(\Lambda) + I_{NPC\_q}\sin(\Lambda)\right)(\delta-\eta) \quad (7)$$

where [6]

$$I_{NPC\_d} = 2Re\{\langle i_{NPC\_a}\rangle_1\} \quad (8)$$

$$I_{NPC\_q} = 2Im\{\langle i_{NPC\_a}\rangle_1\} \quad (9)$$

$$V_{gd} = 2\,Re\{\langle v_{ga}\rangle_1\} \quad (10)$$

$$V_{gq} = 2\,Im\{\langle v_{ga}\rangle_1\} \quad (11)$$

$$\Lambda = \left(\theta - \frac{\pi}{2}\right). \quad (12)$$

The state model defined by (4-7) can be rewritten in the more compact form given by:

$$\dot{x}(t) = f\left(x(t), u_p(t), w(t)\right) \quad (13)$$

where

$x(t) = \left[I_{NPC\_d} \quad I_{NPC\_q} \quad \left(V_{bus\_1}+V_{bus\_2}\right) \quad \left(V_{bus\_1}-V_{bus\_2}\right)\right]^T$ is the state space vector, $w(t) = [V_{gd} \quad V_{gq}]^T$ is the measurable disturbances vector and $u_p(t) = [M \quad \Lambda \quad \delta \quad \eta]^T$ is the virtual control vector.

Remark 2

i. According to the virtual control vector $u_p(t)$, the actual switching functions are constructed in accordance with (1,2).

ii. By performing the following notations:

$$V_{NPC\_d} = \left[V_{bus\_1}\left(\frac{M}{2}+\frac{2\delta}{\pi}\right) + V_{bus\_2}\left(\frac{M}{2}+\frac{2\eta}{\pi}\right)\right]\cos(\Lambda) \quad (14)$$

$$V_{NPC\_q} = \left[V_{bus\_1}\left(\frac{M}{2}+\frac{2\delta}{\pi}\right) + V_{bus\_2}\left(\frac{M}{2}+\frac{2\eta}{\pi}\right)\right]\sin(\Lambda) \quad (15)$$

one can easily show that the control parameters Λ and M verify:

$$\Lambda = \tan^{-1}\left(\frac{V_{NPC\_q}}{V_{NPC\_d}}\right) \quad (16)$$

$$M = \frac{2}{V_{bus\_1}+V_{bus\_2}}\left(\sqrt{{V_{NPC\_d}}^2 + {V_{NPC\_q}}^2} - \frac{2\delta}{\pi}V_{bus\_1} - \frac{2\eta}{\pi}V_{bus\_2}\right) \quad (17)$$

IV. GRID CONNECTED PHOTOVOLTAIC SYSTEM CONTROL DESIGN

A. Reformulation of control objectives

For the grid connected photovoltaic system described in Fig.1, we are aiming for the achievement of the following control objectives:

i. Controlling the transmitted photovoltaic power (P_{pv}) to the grid.

ii. Keeping constant the DC bus voltage (V_{bus}).

iii. Balancing the capacitor voltages (V_{bus_1}, V_{bus_2}).

iv. Controlling the NPC AC currents (I_{NPC_d}, I_{NPC_q}) for reactive power compensation and load current harmonics suppression.

The control system involves just two control inputs (the d and q components of the switching functions $(sw_{(d,q)})$. However, there are four variables that need to be controlled ($I_{NPC\_d}, I_{NPC\_q}, V_{bus}$ and $\left(V_{bus\_1}-V_{bus\_2}\right)$). Thus, the idea will be to design a cascade control which involves two control loops (see Fig.2). The outer control loop aims to regulate the DC bus voltage and to balance the capacitor voltages (V_{bus_1}, V_{bus_2}). The outer loop controller adjusts the DC components of the NPC inverter control signals (denoted $(\delta\,, \eta)$). The signals generated by the outer loop are then used to construct the desired fundamental active components (denoted by: $(i_{pa}\,, i_{pb}\,, i_{pc})$) of the inverter output current. These fundamental components, computed according to the available PV power, are completed with the load current harmonic and reactive components (respectively denoted by: $I_{NL\_hr_d}, I_{NL\_hr_q}$), to develop the final AC current references: $(I^*_{NPC\_d}\,, I^*_{NPC\_q})$ [13]. The inner control loop aims to track the reference signals of the inverter AC current. The inner loop controller adjusts the control parameters (M, Λ) of the NPC inverter. According to (1,2), and with the control vector parameters $[M \quad \Lambda \quad \delta \quad \eta]^T$ one can compute the switching functions $(sw_{(a,b,c)})$ (see Fig.2).

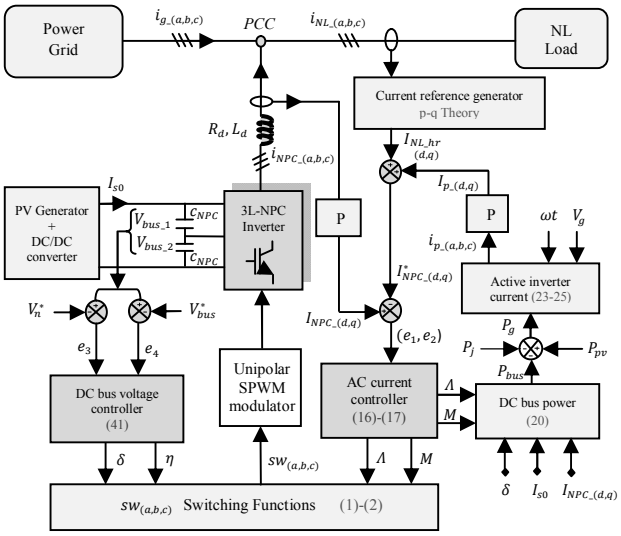

Figure 2. Signals Flow In The Proposed Control Strategy.

B. AC currents references construction

With the notations defined in Table I and Figs.(1,2), the recovered power at the AC side of the NPC inverter (P_{NPC}) is given by:

$$P_{NPC} = V_{NPC\_d}I_{NPC\_d} + V_{NPC\_q}I_{NPC\_q} = \left(V_{gd}I_{NPC\_d} + V_{gq}I_{NPC\_q}\right) - P_{joul} \quad (18)$$

where $P_{joul} = \underbrace{R_d\left(I^2_{NPC\_d} + I^2_{NPC\_q}\right)}_{Joule's\ losses}$ presents Joule's losses at the decoupling filter.

Elsewhere, the DC bus control requires a DC power denoted by (P_{bus}), and defined by:

$$P_{bus} = \underbrace{C_{NPC}\frac{d(V_{bus\_1}+V_{bus\_2})}{dt}}_{P_c} + \underbrace{C_{NPC}\frac{d(V_{bus\_1}-V_{bus\_2})}{dt}}_{P_b} \quad (19)$$

where P_c and P_b correspond respectively to the required power for adjusting the DC bus voltage and for balancing the capacitor voltages.

By substituting (6) and (7) in (19) one has:

$$P_{bus} = 2\langle I_{s0}\rangle_0 - \frac{3}{2}M\left(I_{NPC\_d}\cos(\Lambda) + I_{NPC\_q}\sin(\Lambda)\right) - \frac{6}{\pi}\left(I_{NPC\_d}\cos(\Lambda) + I_{NPC\_q}\sin(\Lambda)\right)\delta. \quad (20)$$

Let us note by P_{pv} the extracted optimal power from the PVG. By performing a power balance, one can easily obtain:

$$P_{pv} = P_{NPC} + P_{bus}. \quad (21)$$

By using (18) and (21), the available electrical power at the PCC (denoted by P_g) is given by:

$$P_g = P_{pv} - P_{bus} - P_{joul}. \quad (22)$$

With (22), one can easily deduce the desired fundamental active components (i_{pa}, i_{pb}, i_{pc}) for the injected current at the PCC. Indeed, with $\omega = 2\pi f_s$ (rad/s) one has:

$$i_{pa} = \frac{P_g}{3V_g}\sqrt{2}cos\,(\omega t) \quad (23)$$

$$i_{pb} = \frac{P_g}{3V_g}\sqrt{2}cos\,(\omega t - 2\pi/3) \quad (24)$$

$$i_{pc} = \frac{P_g}{3V_g}\sqrt{2}cos\,(\omega t - 4\pi/3). \quad (25)$$

Now by using Park transformation one can construct from (23-25), the d and q components (I_{pd}, I_{pq}) for the triphase current (i_{pa}, i_{pb}, i_{pc}).

According to the structure of the proposed cascade control (illustrated by Fig.2), the NPC current references $(I^*_{NPC\_d}, I^*_{NPC\_q})$ are given by:

$$\begin{bmatrix} I^*_{NPC\_d} \\ I^*_{NPC\_q} \end{bmatrix} = \begin{bmatrix} I_{pd} \\ I_{pq} \end{bmatrix} + \begin{bmatrix} I_{NL\_hr_d} \\ I_{NL\_hr_q} \end{bmatrix} \quad (26)$$

where the load current harmonic and reactive components $(I_{NL\_hr_d}, I_{NL\_hr_q})$ are extracted using the instantaneous active and reactive power technique (p-q Theory) [13].

C. Current controller design

The inner control loop is designed to track the current references $(I^*_{NPC\_d}, I^*_{NPC\_q})$ (see Fig.2). This loop must be able to ensure the convergence of the following current tracking errors to zero:

$$e_1 = I_{NPC\_d} - I^*_{NPC\_d} \quad (27)$$

$$e_2 = I_{NPC\_q} - I^*_{NPC\_q}. \quad (28)$$

To this end, using (4) and (5), time derivative of the tracking error vector $[e_1\ e_2]^{\mathrm{T}}$ is given by the following equation:

$$\begin{bmatrix} \dot{e}_1 \\ \dot{e}_2 \end{bmatrix} = -\frac{R_d}{L_d}\begin{bmatrix} I_{NPC\_d} \\ I_{NPC\_q} \end{bmatrix} + \omega\begin{bmatrix} I_{NPC\_q} \\ -I_{NPC\_d} \end{bmatrix} - \frac{1}{L_d}\begin{bmatrix} V_{gd} \\ V_{gq} \end{bmatrix} + \frac{1}{L_d}\begin{bmatrix} V_{NPC\_d} \\ V_{NPC\_q} \end{bmatrix} - \begin{bmatrix} \frac{dI^*_{NPC\_d}}{dt} \\ \frac{dI^*_{NPC\_q}}{dt} \end{bmatrix} \quad (29)$$

where both the virtual controls V_{NPC_d} and V_{NPC_q} are respectively defined by (14,15).

In order to guarantee the convergence of the error vector $[e_1\ e_2]^{\mathrm{T}}$ to $[0\ 0]^{\mathrm{T}}$, the virtual control (V_{NPC_d}, V_{NPC_q}) must be chosen so that:

$$-\begin{bmatrix} k_1e_1 \\ k_2e_2 \end{bmatrix} = -\frac{R_d}{L_d}\begin{bmatrix} I_{NPC\_d} \\ I_{NPC\_q} \end{bmatrix} + \omega\begin{bmatrix} I_{NPC\_q} \\ -I_{NPC\_d} \end{bmatrix} - \frac{1}{L_d}\begin{bmatrix} V_{gd} \\ V_{gq} \end{bmatrix} + \frac{1}{L_d}\begin{bmatrix} V_{NPC\_d} \\ V_{NPC\_q} \end{bmatrix} - \begin{bmatrix} \frac{dI^*_{NPC\_d}}{dt} \\ \frac{dI^*_{NPC\_q}}{dt} \end{bmatrix} \quad (30)$$

where k_1, k_2 are any real positive control design parameters.

By solving (30) with respect to (V_{NPC_d}, V_{NPC_q}) the virtual control is obtained as follows:

$$\begin{bmatrix} V_{NPC\_d} \\ V_{NPC\_q} \end{bmatrix} = -L_d\begin{bmatrix} k_1e_1 \\ k_2e_2 \end{bmatrix} + R_d\begin{bmatrix} I_{NPC\_d} \\ I_{NPC\_q} \end{bmatrix} + \begin{bmatrix} V_{gd} \\ V_{gq} \end{bmatrix} - L_d\omega\begin{bmatrix} I_{NPC\_q} \\ -I_{NPC\_d} \end{bmatrix} + L_d\begin{bmatrix} \frac{dI^*_{NPC\_d}}{dt} \\ \frac{dI^*_{NPC\_q}}{dt} \end{bmatrix}. \quad (31)$$

Replacing (31) in (29), the time derivative of the error vector $[e_1\ e_2]^{\mathrm{T}}$ will be undergoing the following equation:

$$\begin{bmatrix} \dot{e}_1 \\ \dot{e}_2 \end{bmatrix} = -\begin{bmatrix} k_1e_1 \\ k_2e_2 \end{bmatrix}. \quad (32)$$

With (31), the virtual control parameters $(\Lambda,\ M)$ are respectively computed by (16-17).

D. DC bus controller design

The outer loop seeks to force the following tracking errors at asymptotically vanishing:

$$e_3 = (V_{bus\_1} - V_{bus\_2}) - V^*_n \quad (33)$$

$$e_4 = (V_{bus\_1} + V_{bus\_2}) - V^*_{bus}. \quad (34)$$

The reference signal (V^*_n) is kept equal to zero for balancing the capacitor voltages $(V_{bus\_1},\ V_{bus\_2})$. The signal (V^*_{bus}) constitutes the reference value of the DC bus voltage.

By using the tracking errors system given by (33,34), the considered sliding surface is defined by [14,15]:

$$S = \begin{bmatrix} S_1 \\ S_2 \end{bmatrix} = \begin{cases} k_3e_3 + \int k_{30}e_3 \\ k_4e_4 + \int k_{40}e_4 \end{cases} \quad (35)$$

where k_3, k_{30}, k_4, k_{40} are any real positive control design parameters.

The outer loop purpose is to force the sliding surfaces to converge to 0. By using (6,7), the sliding surface dynamic will take the following form:

$$\dot{S} = F + D\begin{bmatrix} \delta - \eta \\ \delta + \eta \end{bmatrix} \quad (36)$$

where

$$F = \begin{bmatrix} k_{30}(V_{bus\_1} - V_{bus\_2}) \\ k_4\frac{2}{C_{NPC}}\langle I_{s0}\rangle_0 - k_4\frac{3}{2C_{NPC}}M(I_{NPC\_d}\cos(\Lambda) + I_{NPC\_q}\sin(\Lambda)) \\ -k_4\dot{V}^*_{bus} + k_{40}(V_{bus\_1} + V_{bus\_2}) - k_{40}V^*_{bus} \end{bmatrix} \quad (37)$$

$$D = \begin{bmatrix} -\frac{3k_3}{\pi C_{NPC}}(I_{NPC\_d}\cos(\Lambda) + I_{NPC\_q}\sin(\Lambda)) & 0 \\ 0 & -\frac{3k_4}{\pi C_{NPC}}(I_{NPC\_d}\cos(\Lambda) + I_{NPC\_q}\sin(\Lambda)) \end{bmatrix}. \quad (38)$$

Equation (36) shows that the sliding surface S can be controlled by the virtual vector input $[\delta\ \ \eta]^{\mathrm{T}}$. Thus, the objective is to determine the considered control vector to ensure the attractiveness and invariance of the surface S $(S = 0)$.

Let us consider for the tracking errors system (33,34) the following Lyapunov's candidate function [14,15]:

$$V_a = \frac{1}{2}S^TS. \quad (39)$$

By using (36), the time derivative of the considered Lyapunov's function takes the following form:

$$\dot{V}_a = S^T\dot{S} = S^T\left(F + D\begin{bmatrix} \delta - \eta \\ \delta + \eta \end{bmatrix}\right). \quad (40)$$

Equation (40) suggests choosing the virtual control vector $[\delta\ \ \eta]^{\mathrm{T}}$ as follows:

$$\begin{bmatrix} \delta - \eta \\ \delta + \eta \end{bmatrix} = -D^{-1}F - D^{-1}\begin{bmatrix} d_1sign(S_1) \\ d_2sign(S_2) \end{bmatrix} \quad (41)$$

where d_1, d_2 are any real positive control design parameters.

V. SIMULATION RESULTS

A. Simulation protocol

The simulations are conducted on MATLAB environment. The considered grid connected PV system is that described by Fig.1. Indeed, the considered nonlinear load is constituted by an AC/DC converter with a *RL* load. The PVG is connected to the power grid through a DC/DC converter and a 3-level NPC inverter. The latter functions on the basis of the SPWM with a switching frequency of $8\,kHz$. The nonlinear load and PV/Grid characteristics are gathered in Table II.

Table II. PV/Grid characteristics

System	Parameter	Value	
NPC Inverter	level	3	
	C_{NPC}	$6.6\,x\,10^{-6}$	F
Decoupling Filter	L_d	$2\,x\,10^{-3}$	H
	R_d	$12\,x\,10^{-3}$	Ω
Nonlinear Load	L_r	$10\,x\,10^{-3}$	H
	R_r	130	Ω
Power Grid	V_g	220	V
	f_g	50	Hz

In this section, for the considered multilevel inverter, the proposed control system is evaluated. To assess the control system performances at different operation points, the solar irradiance parameter (λ) is made variable, according to the profile described by Fig.3. In fact, the simulation protocol is designed in such a way to consider a large variation of the mean solar irradiance ($400-1100\,w/m^2$). For the simulation, the PVG is represented by its familiar physical model (single diode model) [6,34]. The DC/DC converter control (for MPPT) is performed by using P&O algorithm [6]. The resulting PVG optimal power is presented in Fig.4.

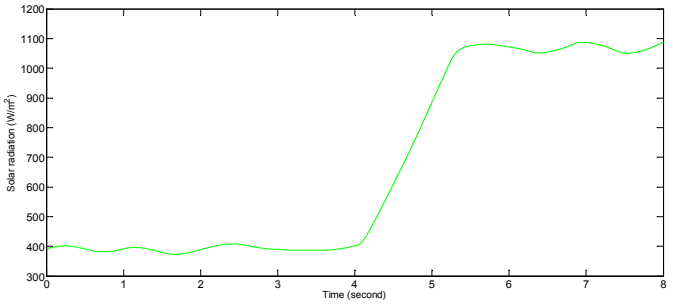

Figure 3. Solar Irradiance Profile (λ) In (W/m^2).

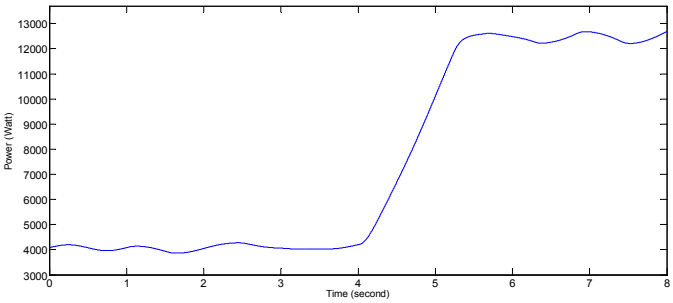

Figure 4. Optimal Available PVG Power (P_{pv}) In (W) According To The Considered Solar Irradiance Profile.

Moreover, to evaluate the performances of the developed controllers at different operation points, the load resistance (R_r) is made variable as follows: $130\,\Omega$ for $t \in [0\ s\ \ 2.5\ s]$, and $29.4\,\Omega$ for $t \in [2.5\ s\ \ 8\ s]$. The resulting load current is plotted in Fig.5.

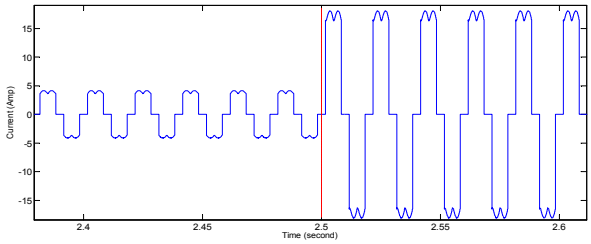

Figure 5. Load Current Phase-a (i_{NL_a}) In (A).

B. Control system performances evaluation

The proposed control system includes the AC current controller (16,17) and the DC bus voltage controller (41). The corresponding design parameters are given in Table III. These parameters turn out to be suitable for the controllers.

Table III. Control system parameters

AC current controller	k_1	$5\,x\,10^3$	DC voltage controller	k_3	$4\,x\,10^2$
	k_2	$6\,x\,10^3$		k_{30}	$1\,x\,10^2$
				k_4	$5\,x\,10^2$
				k_{40}	$1\,x\,10^2$
				d_1	$0.8\,x\,10^2$
				d_2	$1\,x\,10^2$

a) Inner loop evaluation

The resulting control system performances are illustrated by Figs.(6-9). In fact, Fig.6 and Fig.7 show that, independently of the load current and solar irradiance level, the NPC output AC currents track well their references. Fig.8 describes the power flow exchange between the PV system and the power grid. This power exchange remains balanced with the load power variation. Fig.9 shows that the proposed control system forces the grid current to be in phase (or in phase opposition) with the grid voltage. This confirms the perfect compensation of the load reactive power. Indeed, The resulting grid current is plotted in Fig.9. It clearly appears that this current is clean of harmonics (1.12 % for grid current THD rather than 32.6 % for load current THD). This confirms that the PV system can also contribute greatly in improving the quality of the supplied energy.

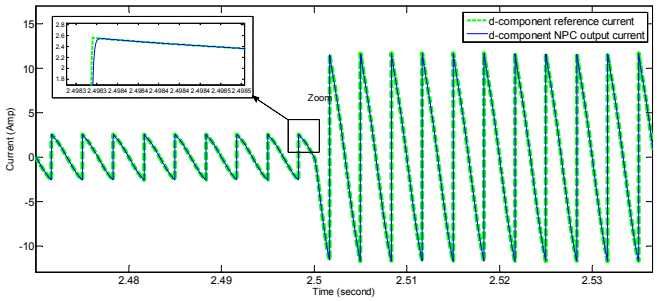

Figure 6. Inner Loop Performances. Solid Line: d-Component Of The NPC Output Current (I_{NPC_d}). Dashed Line: Its Reference Signal ($I^*_{NPC\_d}$) In (A).

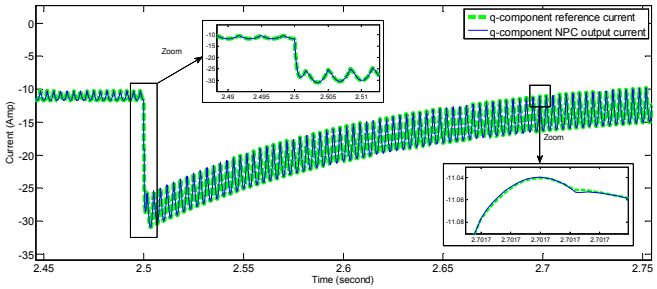

Figure 7. Inner Loop Performances. Solid Line: q-Component Of The NPC Output Current (I_{NPC_q}). Dashed Line: Its Reference Signal ($I^*_{NPC\_q}$) In (A).

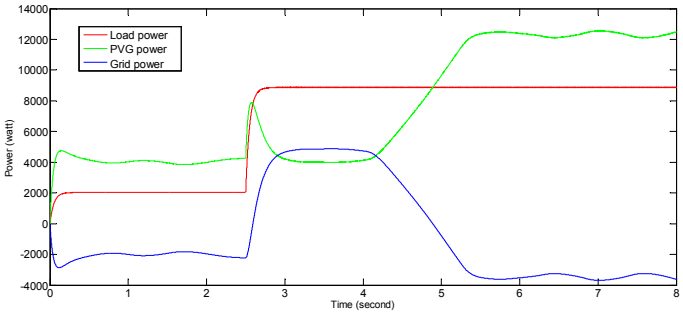

Figure 8. PV/Grid Power Flow In (W).

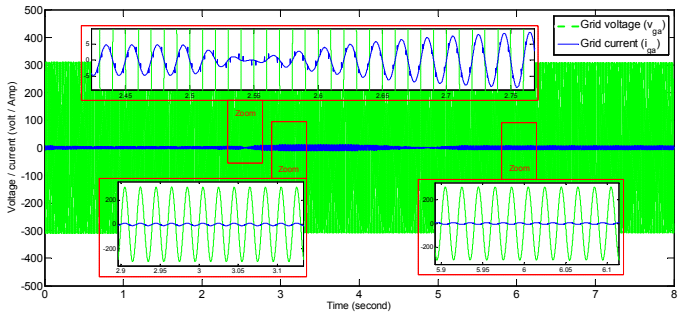

Figure 9. Grid Voltage And Current. Solid Line: Grid Current Phase-a (i_{ga}) in (A). Dashed Line: Grid Voltage Phase-a (v_{ga}) In (V).

b) Outer loop evaluation

For the outer control loop, the voltage references (V_{bus}^*, V_n^*) are respectively kept equal to $200\,V$ and $0\,V$. The DC bus controller performances are illustrated by Figs.(10,11). Indeed, Fig.10 shows that the DC bus voltage tracks well its reference signal. Likewise, Fig.11 shows that the voltage difference $(V_{bus\_1} - V_{bus\_2})$ exponentially vanishes.

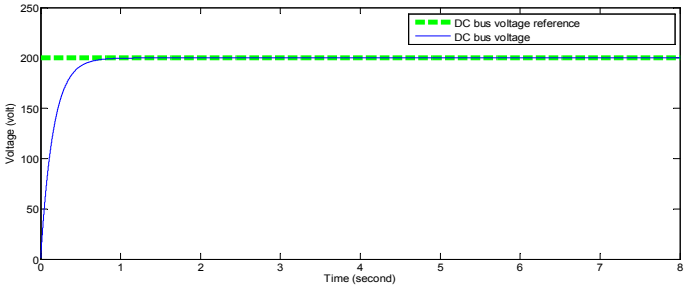

Figure 10. Outer Loop Performances. Solid Line: DC Bus Voltage (V_{bus}) In (V). Dashed Line: Its Reference Signal (V_{bus}^*) In (V).

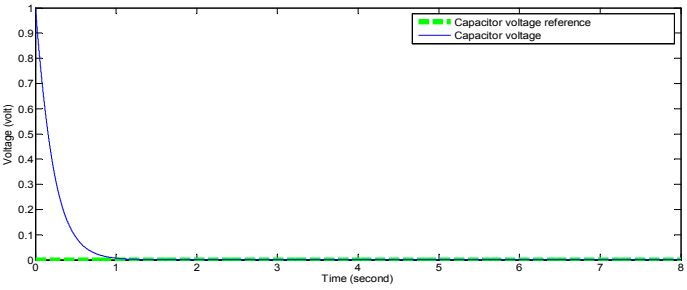

Figure 11. Outer Loop Performances. Solid Line: The Capacitor Voltage Difference $(V_{bus\_1} - V_{bus\_2})$ In (V). Dashed Line: Its Reference Signal (V_n^*: Zero Voltage) In (V).

VI. CONCLUSION

In this paper, a new nonlinear control for three phase grid connected PV system (described by Fig.1) was designed. The considered control objectives have been threefold: (*i*) injecting the PVG power into the grid; (*ii*) compensating the reactive power and cancelling the current harmonics generated by nonlinear loads; (*iii*) regulating the DC bus voltage and keep the balance of the capacitive divider. To meet these objectives, two nonlinear closed-loops have been developed based on a generalized average model of the NPC inverter. The control system includes: Firstly, the AC current controller (16,17) which was designed with the Backstepping technique. Secondly, the DC bus voltage controller (41) which was designed using sliding mode control technique. The performances of the proposed control system have been validated by several simulations. In fact, whatever the solar irradiance value, the PV system injects the available photovoltaic power into the grid and perfectly contributes to satisfy the variable load power. Furthermore, the PV system improves the power quality by compensating harmonic and reactive currents generated by the nonlinear load.

REFERENCES

[1] R. Teodorescu, M. Liserre, and P. Rodríguez, Grid Converters for Photovoltaic and Wind Power Systems, Wiley, July 2011.

[2] Z. Zeng, H. Yang, R. Zhao, and C. Cheng, "Topologies and control strategies of multi-functional grid-connected inverters for power quality enhancement: A comprehensive review," Renewable and Sustainable Energy Reviews, vol. 24, pp. 223–270, 2013.

[3] S. Chattopadhyay, M. Mitra, and S. Sengupta, Electric Power Quality, Springer, 2011, pp. 17–34.

[4] F. L. Albuquerque, A. J. Moraes, G. C. Guimaraes, S. M. R. Sanhueza, and A. R. Vaz, "Photovoltaic solar system connected to the electric power grid operating as active power generator and reactive power compensator," Solar Energy, vol. 84, pp. 1310–1317, 2010.

[5] S. Khomfoi, and L. M. Tolbert, Power Electronics Handbook. Devices, Circuits, and Applications, 3rd ed, Elsevier, 2011, chap. 17.

[6] A. Yazdani, and R. Iravani, "A Generalized State-Space Averaged Model of the Three-Level NPC Converter for Systematic DC-Voltage-Balancer and Current-Controller Design," IEEE Transactions On Power Delivery, vol. 20, pp. 1105–1114, April 2005.

[7] S. Dasgupta, S. K. Sahoo, and S. K. Panda, "Single-Phase Inverter Control Techniques for Interfacing Renewable Energy Sources With Microgrid–Part I: Parallel-Connected Inverter Topology With Active and Reactive Power Flow Control Along With Grid Current Shaping," IEEE Trans. On Power Electronics, vol. 26, pp. 717–731, March 2011.

[8] G. Tsengenes, and G. Adamidis, "Investigation of the behavior of a three phase grid-connected photovoltaic system to control active and reactive power," Electric Power Systems Research, vol. 81, pp. 177–184, 2011.

[9] A. Ravi, P. S. Manoharan, and J. V. Anand, "Modeling and simulation of three phase multilevel inverter for grid connected photovoltaic systems," Solar Energy, vol. 85, pp. 2811–2818, 2011.

[10] S. Sezen, A. Aktas, M. Ucar, and E. Ozdemir, "A three-phase three-level NPC inverter based grid-connected photovoltaic system with active power filtering," 16th International Power Electronics and Motion Control Conference and Exposition, Antalya, Turkey, 21–24 Sept 2014.

[11] G. Vázquez, P. Rodriguez, R. Ordoñez, T. Kerekes, and R. Teodorescu, "Adaptive Hysteresis Band Current Control for Transformerless Single-Phase PV Inverters," 35th Annual Conference of IEEE Industrial Electronics, 2009.

[12] E. Pouresmaeil, O. Gomis-Bellmunt, D. Montesinos-Miracle, and J. Bergas-Jané, "Multilevel converters control for renewable energy integration to the power grid," Energy, vol. 36, pp. 950–963, 2011.

[13] H. Ouadi, A. Ait Chihab, F. Giri, "Adaptive nonlinear control of three-phase shunt active power filters with magnetic saturation," Electrical Power and Energy Systems, vol. 69, pp. 104–115, 2015.

[14] J. J. E. Slotine, and W. Li, Applied Nonlinear Control, Prentice-Hall, 1991.

[15] W. Perruquetti, and J. P. Barbot, Sliding mode control in engineering, Marcel Dekker, 2002.